Available online at www.sciencedirect.com
ScienceDirect
Trans. Nonferrous Met. Soc. China 32(2022) 3714−3730
Transactions of Nonferrous Metals Society of China
www.tnmsc.cn

Dynamic compressive strength and failure mechanisms of microwave damaged sandstone subjected to intermediate loading rate

Pin WANG[1,2], Tu-bing YIN[1], Xi-bing LI[1], Heinz KONIETZKY[2]

1. School of Resources and Safety Engineering, Central South University, Changsha 410083, China;
2. Geotechnical Institute, TU Bergakademie Freiberg, Freiberg, 09596, Germany

Received 27 August 2021; accepted 6 April 2022

Abstract: To investigate the influence of microwave heating on the dynamic behavior and failure mechanisms of rock, dynamic compression tests were conducted on microwave-irradiated sandstone specimens using a modified split Hopkinson pressure bar (SHPB) system. Experimental results show that microwave radiation can effectively weaken the compressive strength of sandstone. Rock specimens show three different failure modes under impact load: tensile failure, tensile−shear composite failure and compressive−shear failure. The dynamic Poisson's ratio, calculated using the measured P- and S-wave velocities, is introduced to describe the deformation characteristics of sandstone. With the increase in microwave power and heating time, the Poisson's ratio declines first and then increases slightly, and the turning point occurs at 244.6 °C. Moreover, the microstructural characteristics reveal that microwave radiation produces dehydration, pore expansion, and cracking of the rock. The damage mechanisms caused by microwave radiation are discussed based on thermal stress and steam pressure inside the rock, which provides a reasonable explanation for the experimental results.

Key words: sandstone; microwave radiation; thermal cracking; dynamic compressive strength; failure patterns; split Hopkinson pressure bar

1 Introduction

Rock extraction and crushing are core activities in several industries like mining, tunneling, process engineering or drilling. Blasting and mechanical extraction are by far the most popular excavation methods used in rock engineering. Blasting causes a more extensive disturbance (fracturing) to the rock mass and generates a lot of dust and noise (pollution of the environment) [1,2]. It also has limits to create precise opening contours. Especially in areas with high-stress levels, blasting can induce rockburst disasters [3]. Therefore, the mechanical extraction method has increasing usage (more accurate operation, less environmental impact, high degree of automation, continuous construction etc). However, mechanical extraction also has some weak points like severe tool wear, high energy consumption, high initial investment and maintenance costs [4−6]. To address these problems, new or modified rock breaking methods are under investigation, such as high-pressure water jet cutting [7,8], ultrasonic methods [9], spark discharge methods [10], laser-plasma methods [11], and microwave methods [12−14]. Using the above-mentioned methods to pre-crack the rock can reduce the strength and frictional resistance of the rock, thereby improving the efficiency of the mechanical extraction process.

Microwave irradiation heats up the rock internally and produces thermal damage. It is characterized by fast heating, high efficiency, strong

Corresponding author: Tu-bing YIN, Tel: +86-18684770361, E-mail: tubing_yin@csu.edu.cn
DOI: 10.1016/S1003-6326(22)66052-7

penetration (but limited depth), and easy control of the heating process. Already in 1979, GUSHCHIN et al [15] designed a roadheader with an integrated microwave tool for phosphate mining tests. In 1984, PROTASOV et al [16] carried out tunnel boring tests with a 380 kW combined microwave mechanical roadheader. Their results showed that the combined application of microwave and mechanical rock breaking has the potential to be an efficient and less expensive extraction method compared with the classical ones. Besides, many laboratory tests have been conducted to investigate the influence of microwave irradiation on the degradation of mechanical properties of rocks, including uniaxial compressive strength tests [17], point load tests [18], tensile strength tests [19], fracture toughness tests [20,21], and cutting force tests [22]. It is generally accepted that microwave irradiation weakens mechanical strength. The change of mechanical properties mainly depends on microwave power density and exposure time, mineral composition and particle size of the rock, and the presence of water [23−25]. Under the same irradiation energy, the combination of high heating power and little heating time is more effective to destroy rocks [26,27].

However, all of the mechanical properties mentioned above are deduced from static tests. In fact, in the process of mechanical drilling, the cutter head and rock are in a complex interaction, usually at medium to high strain rates [28,29]. As a strain rate sensitive material, the mechanical properties of rock under dynamic load are quite different from those under static load [30]. To examine the effect of microwave radiation on dynamic mechanical properties, KINGMAN et al [31] investigated the influence of microwave radiation on ore crushing. They reported that the irradiated lead−zinc ore becomes more fragile when subjected to impact loading, and the required crushing energy for the ore was reduced. RIZMANOSKI [32] used the drop-weight impact test to study the impact resistance of irradiated rocks. The results showed that microwave radiation could significantly reduce the dynamic strength of rocks. ZHU et al [33] conducted dynamic compression tests on microwave heated granite and studied the influence of water on the deformation and failure process. WANG et al [34] used the split Hopkinson pressure bar system to test irradiated granite samples to simulate the rock crushing process. Their results indicated that the fragmentation degree of rocks is determined by both microwave irradiation time and loading rate. These studies emphasize that the impact resistance and crushing characteristics of irradiated rocks as well as dynamic strength degradation and its underlying damage mechanisms are still not systematically investigated. Moreover, previous research has been primarily focused on changes in the physical and mechanical properties of different igneous rocks after microwave heating, such as basalt [35], granite [36] and gabbro [37], which are all microwave sensitive rocks. The microwave-assisted rock breaking of microwave insensitive rocks still remains an open question.

In this work, the dynamic (impact) behavior of the sandstone as a microwave insensitive material after microwave treatment was considered. The variations in surface temperature, density, wave velocity, dynamic compressive strength, elastic modulus, and axial failure strain of sandstone samples with the change of microwave power and irradiation time were analyzed. Through regression analysis, the corresponding formulas between dynamic compressive strength and applied microwave energy were obtained, which provides a reference for microwave-assisted rock breaking technology.

2 Experimental

2.1 Description of test material

In this study, a relatively homogeneous and isotropic red sandstone from an underground metal mine in Linyi City, Shandong Province, China was selected. The sandstone consists of quartz, feldspar, montmorillonite, mica, hematite, calcite, and some other minerals. The feldspar is mostly K-feldspar and plagioclase, and the mica includes biotite and muscovite. The mass fraction of each mineral component was determined by using X-ray diffraction technology (Fig. 1(a)).

The mineralogical and microstructural characteristics of the sandstone were investigated via optical microscope and scanning electron microscope using different magnifications as shown in Figs. 1(b, c). The clastic content accounts for about 85%, mainly composed of quartz, feldspar, a small amount of rock cuttings and trace opaque minerals. The interstitial content (quartz, calcite and

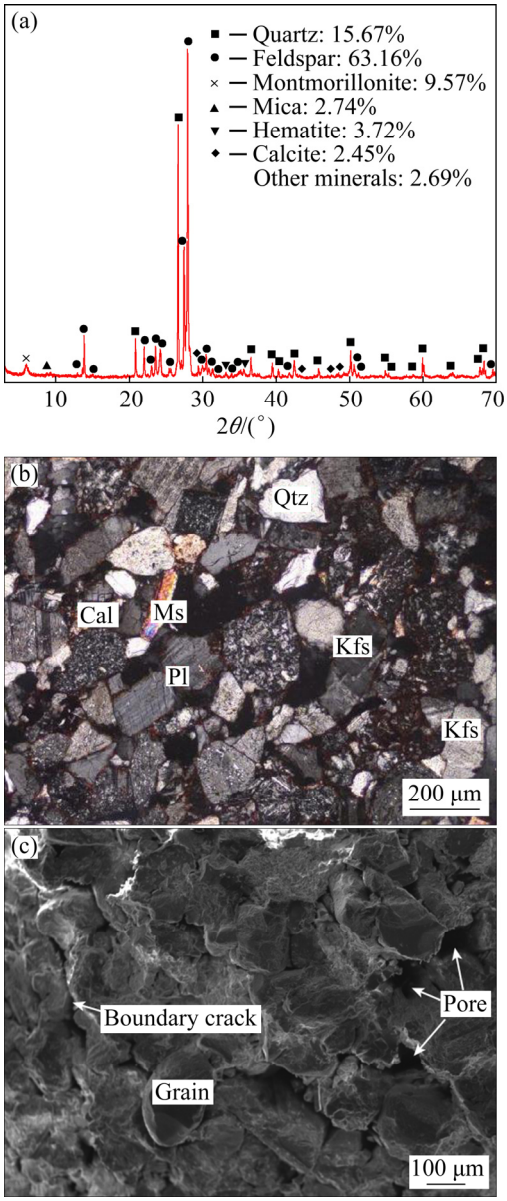

Fig. 1 Mineralogical and microstructural characteristics of sandstone: (a) X-ray diffraction pattern; (b) Optical image; (c) Scanning electron microscope image (Qtz−Quartz; Kfs−Kalium feldspar; Pl−Plagioclase; Cal−Calcite; Ms−Muscovite)

mixed matrix) accounts for about 15%. There cementation consists mainly of porous and locally basal cementation. The mineral particles have a diameter between 0.05 and 0.6 mm. The internal structure is relatively dense, some surface cracks and small pores are detected under the electron microscope.

By using a multi-mode cavity industrial microwave system with frequency of 2.45 GHz and power of 500 W, heating characteristics under microwave irradiation of 14 rock-forming minerals were observed by ZHAO et al [38]. According to the heating rate characteristics, the microwave sensitivity of different minerals was classified. Biotite and hematite are classified as microwave sensitive minerals, while quartz, feldspar and calcite are microwave insensitive minerals. Since the total mass fraction of mica and hematite in tested sandstone is only 6.46 %, the microwave sensitivity of the sandstone samples is relatively low.

2.2 Specimen preparation

The above-mentioned rock material was processed into cylindrical specimens with a diameter of 50 mm and a length to diameter ratio of 1:1. The specific preparation process includes core drilling, cutting and polishing. The accuracy of the specimen met the recommendations of the International Society for Rock Mechanics (ISRM) [39]): unevenness of both ends of the sample is less than 0.02 mm, the end faces are perpendicular to the axis of the specimen with maximum deviation of 0.01 rad. After processing, samples were put into a vacuum drying oven (100 °C for 48 h drying treatment) to prevent the influence of different moisture contents on the dielectric properties of the sample.

Before the microwave irradiation treatment, some basic physical parameters of all dried samples were measured, including mass, density and ultrasonic wave velocities. Samples with large deviation from the average were excluded from further tests. The basic physical and mechanical parameters of the selected samples are listed in Table 1.

2.3 Test setup

2.3.1 Microwave heating system

The microwave heating equipment used in this study is a multi-mode cavity industrial microwave oven (see Fig. 2(a)) produced by Hunan Huaye

Table 1 Physical and mechanical parameters of sandstone (mean value ± standard deviation)

Density, ρ/(kg·m^{-3})	Porosity, ϕ/%	P-wave velocity, V_P/(m·s^{-1})	S-wave velocity, V_S/(m·s^{-1})	Compressive strength, σ_c/MPa	Fracture strain, ε_f/%	Elastic modulous, E_s/GPa	Poisson's ratio, μ
2462.5±2.2	14.96±0.14	3383.2±41.63	1831.6±12.16	96.5±2.33	14.58±0.47	7.49±0.13	0.29±0.01

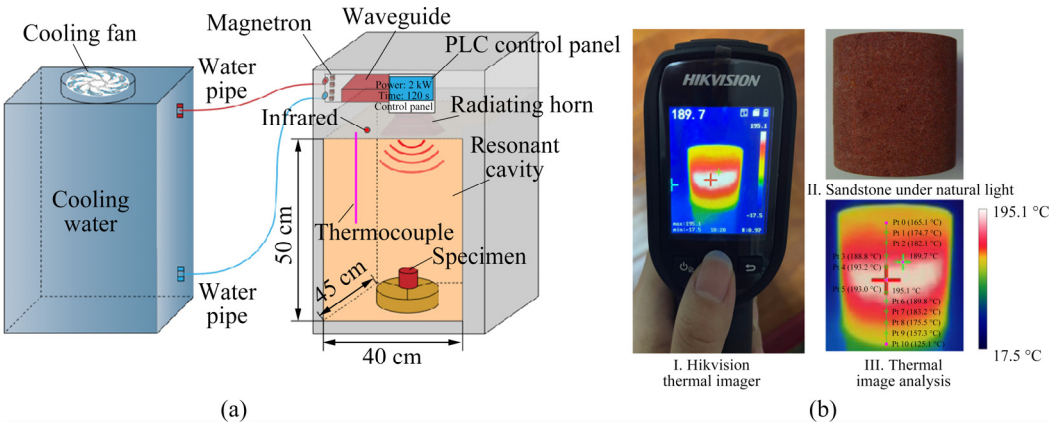

Fig. 2 Schematic diagram of microwave heating system (a) and thermal imaging (b)

Microwave Technology Co., Ltd. (China). The system includes four main parts: microwave heating component, control panel, temperature measuring equipment and cooling system.

The microwave generator is composed of four magnetrons with a maximum output power of 1.5 kW each. The voltage of the equipment is 380 V, microwave frequency is 2.45 GHz, and total maximum microwave output power is 6 kW.

The control system adopts PLC automatic control, which can realize a continuous adjustment of the microwave power (0−6 kW). During the test, the electromagnetic wave is guided by the waveguide and enters the cavity through the radiating horn. The radiating horn is helpful for the uniform distribution of electromagnetic waves in the cavity.

The microwave oven is equipped with a thermocouple and infrared thermometer at the same time. However, because the thermocouple is susceptible to electromagnetic interference, the measurement distance has a greater impact on the accuracy of the infrared thermometer. Therefore, a hand-held infrared thermal imager was used to measure the temperature on the sample surface every 30 s. The infrared thermal imager has high accuracy, distance can easily be controlled, and temperature distribution characteristics of the rock surface can be obtained, as shown in Fig. 2(b).

During the process of microwave irradiation, electromagnetic waves cannot be completely absorbed by the sample, especially by microwave insensitive minerals. Most of the microwave energy is reflected back, which increases the temperature of the magnetron. Therefore, water and a fan were used to cool the magnetron to avoid overheating.

The tests were subdivided into 4 groups according to the microwave radiation power: 1, 2, 3 and 4 kW. The maximum radiation time for each group of samples was 5 min. No less than three rock samples were selected for dynamic mechanical tests.

2.3.2 Split Hopkinson pressure bar

The dynamic compression tests were carried out on the modified split Hopkinson pressure bar system shown in Fig. 3. The main parts of the system are the stress wave loading device, the signal acquisition system and the high-speed camera. The loading device is composed of cone-shaped striker, incident bar, transmission bar and absorption bar, which are all made of 40Cr alloy steel (density of 7810 kg/m^3, Poisson's ratio of 0.28 and elastic longitudinal wave velocity of 5400 m/s). During the test, the sample was placed between incident bar and transmission bar and held in a straight line with the elastic bars. Two pairs of strain gauges were pasted on incident and transmission bar 750 mm away from the sample to record the signals. A high-speed camera was adopted to capture the dynamic failure process of the sample. According to the one-dimensional wave theory, the relationships between stress, strain and strain rate of the specimen can be obtained as follows [40]:

$$\sigma(t)=\frac{A_{\mathrm{e}}E_{\mathrm{e}}}{2A_{\mathrm{s}}}\left[\varepsilon_{\mathrm{I}}(t)+\varepsilon_{\mathrm{R}}(t)+\varepsilon_{\mathrm{T}}(t)\right] \tag{1}$$

$$\varepsilon(t)=\frac{C_{\mathrm{e}}}{L_{\mathrm{s}}}\int_0^t\left[\varepsilon_{\mathrm{I}}(t)-\varepsilon_{\mathrm{R}}(t)-\varepsilon_{\mathrm{T}}(t)\right]\mathrm{d}t \tag{2}$$

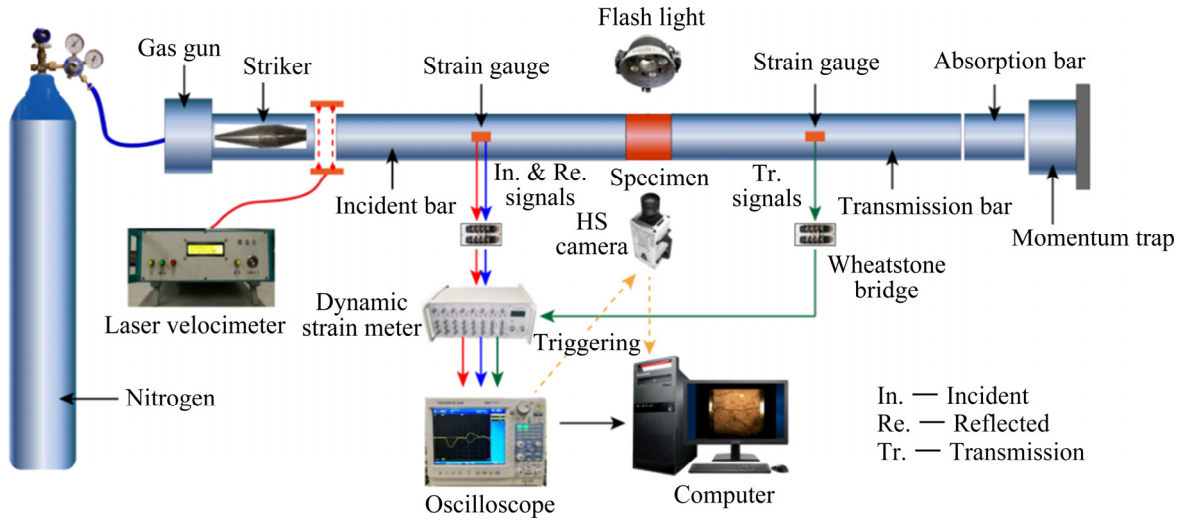

Fig. 3 Schematic diagram of modified split Hopkinson pressure bar system

$$\dot{\varepsilon}(t)=\frac{C_e}{L_s}\left[\varepsilon_I(t)-\varepsilon_R(t)-\varepsilon_T(t)\right] \tag{3}$$

where E_e, C_e and A_e are elastic modulus, longitudinal wave velocity and cross-sectional area of the elastic bars, respectively. L_s and A_s are length and cross-sectional area of the sample, respectively. $\varepsilon_I(t)$, $\varepsilon_R(t)$ and $\varepsilon_T(t)$ are strains of incident, reflected and transmission wave, respectively.

2.3.3 Dynamic force balance

The theoretical basis of a SHPB test is the one-dimensional stress wave theory, and the realization of force balance at both ends of the specimen is the prerequisite to ensure the validity of the test results [41,42]. Therefore, it is necessary to compare the forces at both ends of the specimen. The force non-uniformity coefficient is defined by using Eq. (6) to evaluate the force balance at both ends of the sample.

$$P_1=E_eA_e\left[\varepsilon_I(t)+\varepsilon_R(t)\right] \tag{4}$$

$$P_2=E_eA_e\varepsilon_T(t) \tag{5}$$

$$\eta=\frac{P_1-P_2}{P_2}=\frac{\varepsilon_I(t)+\varepsilon_R(t)-\varepsilon_T(t)}{\varepsilon_T(t)} \tag{6}$$

where P_1 and P_2 are the forces at both ends of the sample, and η is the force non-uniformity coefficient. The closer the value of η to 0, the better the force balance is.

Figure 4 shows a typical stress waveform and the time history of the force non-uniformity coefficient for a dynamic compression test of the sandstone. The stress wave has a half-sine wave shape, and the signal is very smooth. The force non-uniformity coefficient fluctuates strongly at the initial stage, but after the stress wave is reflected back and forth inside the sample, the η value stabilizes and approaches zero. According to our definition, the force equilibrium is reached when η is less than 0.05. As Fig. 4 shows, the force equilibrium is reached before the specimen fails. This state of force equilibrium is maintained until 175 μs, which indicates that the stress−strain relationship after reaching the peak value can reflect the post-peak behavior of the specimen. Figure 5 shows the time history of dynamic stress and the corresponding strain rate. The strain rate curve shows a long plateau near the peak strength, indicating that the spindle-shaped striker can realize a constant strain rate loading of the sample.

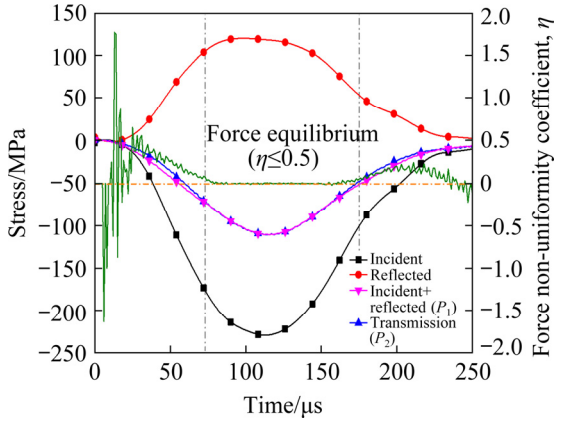

Fig. 4 Typical stress waveform and time history curve of force non-uniformity coefficient

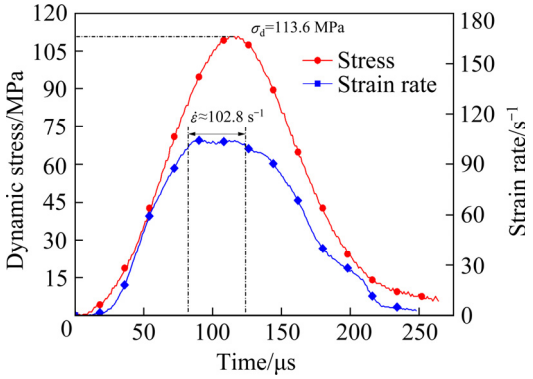

Fig. 5 Time history of dynamic stress and corresponding strain rate

3 Experimental results

3.1 Heating characteristics

With longer irradiation time, the temperature distribution at the sandstone surface becomes similar for different powers of microwave irradiation. Therefore, the thermal images of sandstone samples exposed to 3 kW microwave irradiation power are selected for the analysis, as shown in Fig. 6(a). It becomes visible that before the microwave irradiation time reaches 90 s, the surface temperature shows an obvious gradient from top to bottom because the microwave energy is emitted from the upper radiating horn. With increasing irradiation time, the heat flow leads to a more homogeneous temperature distribution. When the irradiation time reaches 120 s, the center of the sample is bright white and extends to all sides, and the position of the highest temperature is stable at the center of the sample. The main reason for this phenomenon is that the heat dissipation conditions of the rock from the inside to outside are

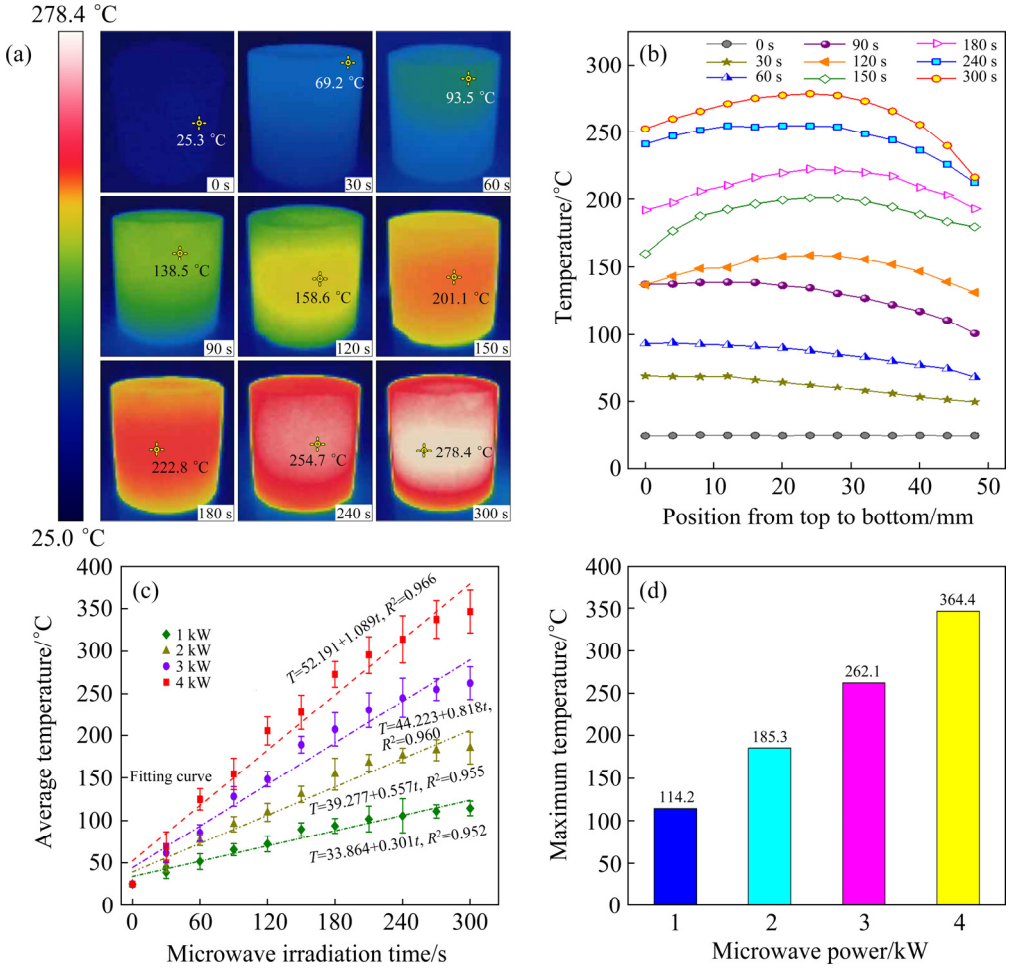

Fig. 6 Variation of surface temperature of sandstone samples exposed to microwave irradiation: (a) Thermal images of sandstone under 3 kW microwave irradiation; (b) Surface temperature distributions along highest temperature point from top to bottom; (c) Average surface temperature for different powers of microwave irradiation; (d) Final surface temperature after microwave heating for 5 min

different, which leads to the temperature in the center of the rock gradually decreasing ring-shapedly toward the edges of the rock.

A measuring line is arranged along the axis of the cylindrical sample passing through the points of the highest temperature on the surface of the sample (Fig. 6(b)). The rising average surface temperature curve of sandstone samples exposed to different microwave powers for 5 min is shown in Fig. 6(c). The rock surface temperature increases linearly with the irradiation time, but the rise is depended on applied irradiation power (Fig. 6(d)). The observed temperature rising characteristics are consistent with the results obtained by LU et al [43].

3.2 Density and ultrasonic wave velocities

During the microwave heat treatment, volume and mass of the sandstone samples were tested every 30 s. The relationship between density and microwave irradiation time is shown in Fig. 7. The density gradually decreases with increase of microwave power and irradiation time. Since the volume of the sandstone samples does not expand during microwave irradiation, it can be inferred that mass loss is the main reason for the decrease in the density of the sandstone.

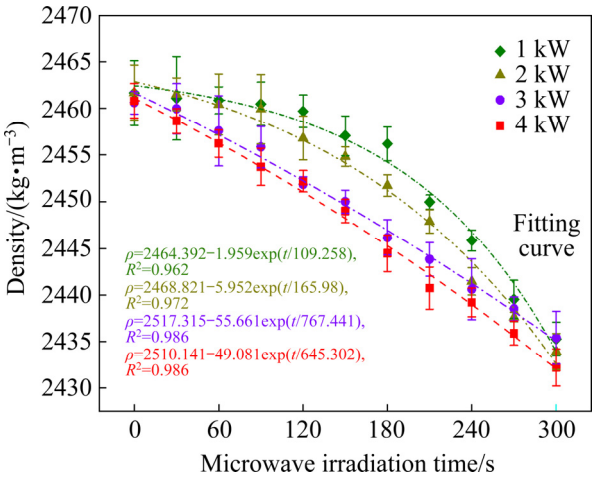

Fig. 7 Variation of sandstone density vs microwave irradiation time and power

However, in this study, all sandstone samples were placed in a vacuum drying oven at 105 °C for 48 h for drying. The state of water in rocks can be divided into free water, adsorption water and bound water. Free and adsorbed water is flowable and can easily evaporate during a conventional oven drying process (105 °C) [44]. However, strongly bonded water, where water molecules are adsorbed on the rock molecules by different polarities with strong bonding potential can only be removed when the rock is heated to temperatures above 105−110 °C. As a strong polar molecule, water has a larger dielectric loss factor, and the heating rate is larger during microwave radiation. Additionally, the rapid rotation and oscillation of the water molecules in the microwave field reduce the adhesion between the water molecules and the rock, so that bond water can easily escape at even lower temperature. Therefore, the decrease of sandstone density under the action of microwave may be related to the escape of stronger bonded water inside the rock.

Under the action of low-power microwaves (1 and 2 kW), the density of sandstone decreases parabolically with microwave irradiation time. In the initial stage of radiation, only the water on the sample surface is lost. Also, because the microwave irradiation time is relatively short, the microwave energy is not enough to destroy the internal structure of the rock in early stage, and the water inside the rock cannot escape. Therefore, the fitting curve shows a gentle inclination in the early stage.

When the microwave power increases to more than 3 kW, the density of sandstone decreases linearly with increasing exposure time. Under the action of high-power microwaves, the heating rate of sandstone increases, and a large number of intergranular cracks are generated inside the rock, which provides channels, so that water inside the rock can escape. This results in an acceleration of the mass loss rate of the sandstone.

Propagation and attenuation characteristics of ultrasonic waves can be used to characterize the development of micro-defects in rocks. Figure 8 shows the evolution of P- and S-wave velocities of sandstone as function of microwave irradiation time and power. With the increase of microwave power and radiation time, longitudinal and transverse wave velocities decrease obviously, which indicates that due to the microwave radiation, a large number of cracks are generated in different directions. Higher radiation power and longer exposure lead to greater damage of the sandstone.

3.3 Dynamic parameters

The stress−strain curves of the rock exposed to different microwave powers and durations are shown in Fig. 9. Different from static compressive

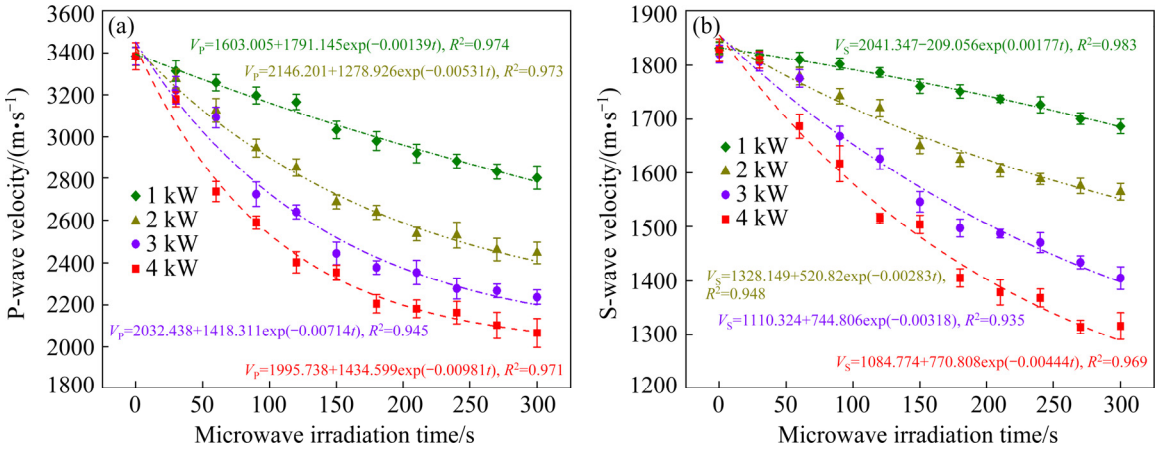

Fig. 8 Variations of P- (a) and S-wave (b) velocities of sandstone exposed to microwave irradiation of different durations and powers

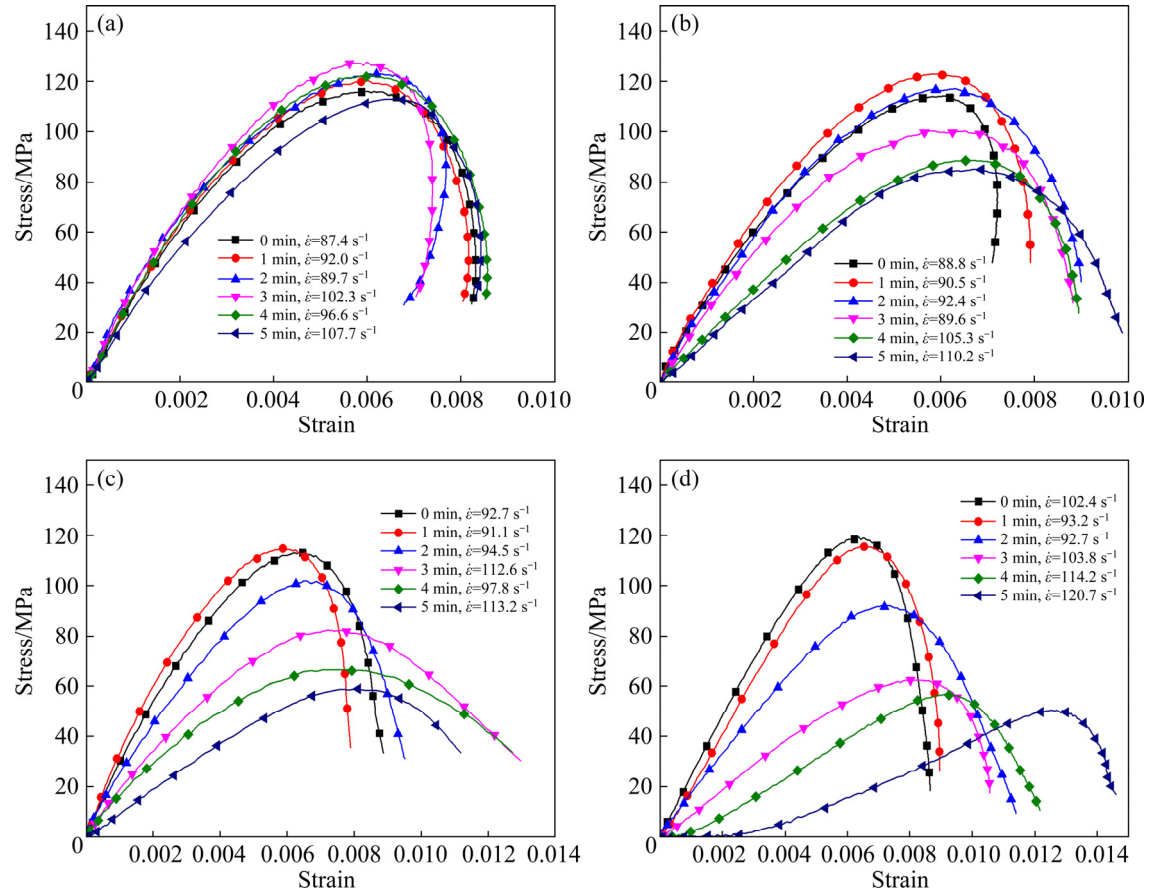

Fig. 9 Stress−strain curves of microwave damaged sandstone under impact loading: (a) 1 kW; (b) 2 kW; (c) 3 kW; (d) 4 kW

testing, the ascending section of the stress−strain curve before the peak does not show a process of micro-crack compaction (closure). This is caused by the rapid loading: the specimen fails before it can go through the compaction stage, which underlines the importance of the loading rate dependence of rock strength.

With the increase of microwave power and the extension of radiation time, the peak stress decreases, the strain increases, the slope before reaching the peak value of the stress−strain curve decreases, and the decline speed of the curve after

the peak becomes slow. All these phenomena indicate that high power and long-term microwave radiation can cause significant damage to the sandstone. Variation of microwave irradiation power alone leads to significantly different dynamic stress−strain curves. Especially under the action of only 1 kW microwave power, the post-peak deformation of the stress−strain curve shows a rebound: strain declines with decreasing the stress. The main reason for this difference may be that the thermal damage caused by microwave is small, and the rock pieces show a partly elastic response (minor damage).

Based on the dynamic stress−strain curves of sandstone presented in Fig. 9, dynamic compressive strength, elastic modulus and peak strain for different microwave powers are obtained and given in Fig. 10. The average value of the dynamic compressive strength of the sandstone before microwave radiation is about 115 MPa, the elastic modulus is approximately 24.5 GPa, and the peak strain is 0.63. The obtained curves can be divided into three parts: 0−90 s, 90−240 s and >240 s.

At the first stage (0−90 s), since the dielectric constant of water is much larger than that of rock, most of the microwave energy is absorbed by the water inside the rock, and the evaporation of water has a cooling effect on the rock. Therefore, thermal damage of the rock caused by microwave radiation is small and the variation of mechanical parameters is not obvious.

During the second stage (90−240 s), with the increase of microwave radiation time, the rock temperature gradually increases and reaches a high value. Due to different heat dissipation from the inside to the outside of the rock and different microwave sensitivity of the mineral particles, a temperature gradient is generated, which results in a significant increase in thermal stress among the mineral particles. At this stage, compressive strength and elastic modulus decrease significantly, while peak strain increases. However, it should be pointed out that strength and elastic modulus of the sandstone do not decrease, but show a slight increase for microwave power of 1 kW. This is related to the low heating level where the expansion of the particles fills the pores without creating significant damage.

At the third stage (240−300 s), the temperature rises with increasing microwave radiation time and inter-crystalline cracks develop with corresponding increase of pore space, which provides conditions for heat dissipation. At this stage, structural thermal stress is reduced and thermal damage rate goes down.

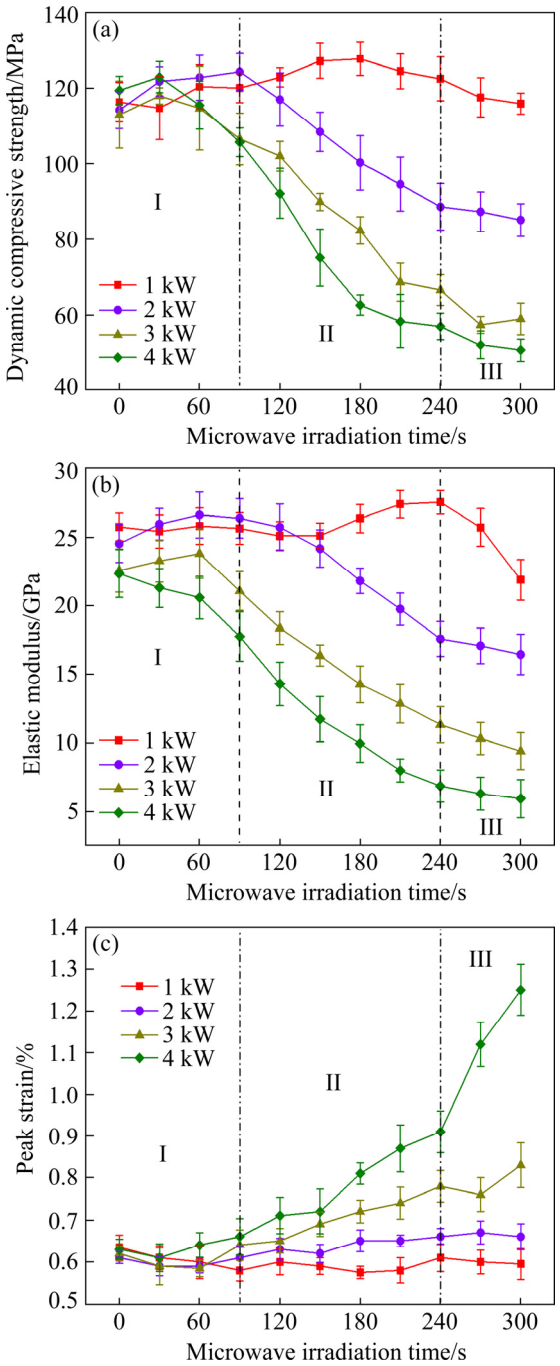

Fig. 10 Variations in dynamic compressive strength (a), elastic modulus (b) and peak strain (c) of sandstone as function of microwave irradiation time

3.4 Fracture behavior and failure modes

The dynamic crack growth and fracture morphology of the sandstone can reflect the thermal

damage and the stress state under the action of external loading. During the test, a Photron SA1.1 high-speed camera was utilized to capture the dynamic failure process of the rock samples. Resolution was set to be 256×128 pixels, actual shooting area was 100 mm × 50 mm, and the acquisition rate was 125000 fps (one photo every 8 μs). Results indicate differences in the crack evolution mode of sandstone under different microwave irradiation conditions. As microwave power increases and irradiation time is prolonged, the failure mode changes from tensile failure to shear failure. The failure process can be roughly divided into three types, as shown in Fig. 11.

Figure 11(a) shows the tensile failure process of sandstone during the dynamic compression test. This failure mode mainly occurs under the conditions of low microwave power and short irradiation time, and the samples maintain high strength and brittleness. At 80 μs, a visible narrow central crack along the loading direction appears. As the dynamic load increases, the crack propagates and expands along the loading axis to both ends of the specimen, and penetrates the entire specimen at 96 μs. At this time, a second parallel crack appears. As the damage develops further and deeper into the sample, the two axial cracks finally split the sample into three pieces. The main reason for this failure mode is that during the rapid loading process, the specimen is laterally unconstrained, and the lateral strain of the sandstone is larger than the longitudinal strain. Transverse strain generates tensile stress perpendicular to the loading direction. When the tensile stress exceeds the tensile strength, the sandstone fails in tension, as shown in Fig. 12(a).

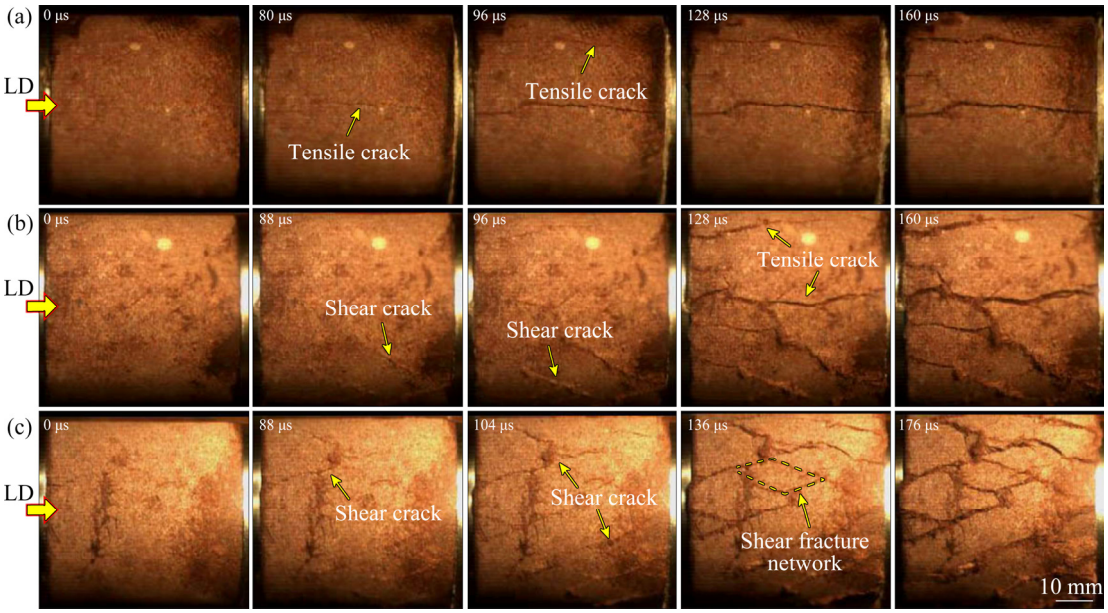

Fig. 11 Typical failure process of sandstone under dynamic compression recorded by HS camera: (a) 2 kW, 90 s; (b) 2 kW, 180 s; (c) 4 kW, 180 s

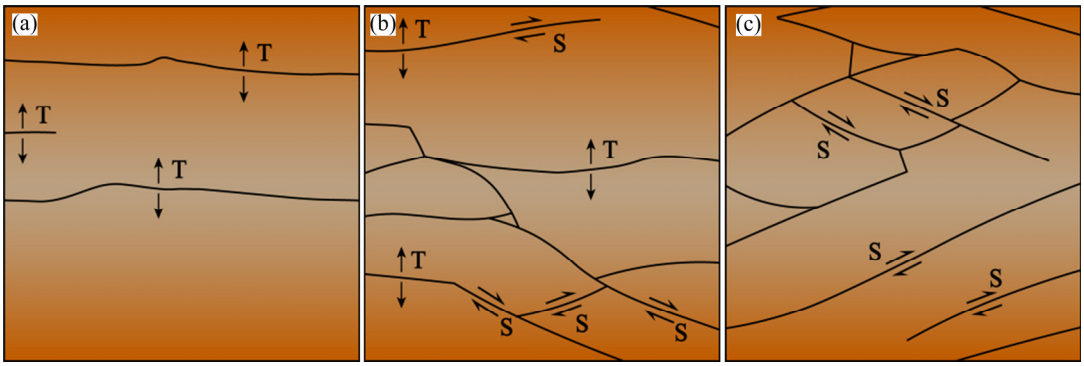

Fig. 12 Different failure modes of sandstone under dynamic compression: (a) Type I: Tensile failure along axial direction; (b) Type II: Tensile−shear composite failure; (c) Type III: Compression−shear failure (T−Tensile; S−Shear)

Figure 11(b) shows tensile−shear composite failure process of sandstone in the dynamic compression test. This failure mode appears under the condition of increased microwave power and prolonged irradiation time. This leads to increased damage, reduced strength and brittleness. The deformation and failure process of the sandstone is controlled by both shear and tensile cracks. However, it is worth noting that in the initial stage of loading, shear cracking is dominant. When loaded to 128 μs, tensile cracking appears. With continuous increase of load, tensile cracks propagate and gradually dominate, which leads to a tensile−shear composite failure pattern dominated by tensile cracks eventually, as shown in Fig. 12(b).

Figure 11(c) shows that the sandstone exhibits a typical compression−shear failure mode under impact load. At the time of 88 μs, shear cracks begin to appear on the surface of the sample. As the load increases, length and number of cracks increase. At 136 μs, an X-shaped slip line appears, forming a shear fracture network, which eventually leads to compression−shear failure of the sample. The final fragmentation is stronger compared to the two previously mentioned cases (see Fig. 12). This failure pattern usually occurs in samples treated with 3 kW microwave power radiated for 4 min and 4 kW microwave power radiated for 3 min or more. One possible explanation for this failure pattern might be that the microwave heating leads to an increase of rock plasticity and change of Poisson's ratio. The decrease in Poisson's ratio is manifested by the decrease in lateral strain, and consequently tensile failure is less likely to occur. This deformation and failure process is closer to that under quasi-static compression.

4 Discussion

4.1 Strength and deformation characteristics

In order to analyze the change of strength under different microwave power conditions, the relationship between dynamic compressive strength and microwave energy is shown in Fig. 13. When the microwave energy is less than 180 kJ, the dynamic compressive strength of sandstone shows a larger scatter, but an increase with increasing microwave energy is visible. In this stage, most of the microwave energy is absorbed by pore water inside the rock. Although the evaporation of pore water contributes to the initiation and expansion of new cracks, the expansion of microwave-sensitive mineral particles leads to an increased rock compactness. When the microwave energy is larger than 180 kJ, the dynamic compressive strength shows a continuous decrease with increasing microwave energy, but the decreasing rate of the curve gradually slows down. On the one hand, with the increase of absorbed microwave energy, different thermal expansion of the microwave sensitive minerals leads to crack growth and fracture evolution related with the reduction in strength. On the other hand, sandstone as a whole is a relatively microwave-insensitive material. With increasing microwave energy input, the energy utilization rate gradually decreases and the strength decreases.

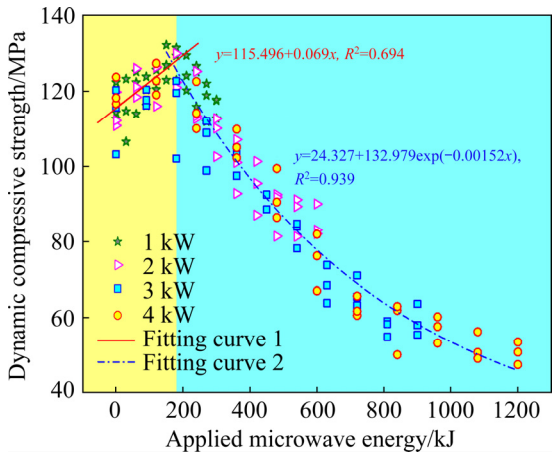

Fig. 13 Dynamic compressive strength vs applied microwave energy for sandstone

The dynamic Poisson's ratio (μ_d) can be derived from the measured P- and S-wave velocities of the rock using the following equation:

$$\mu_d = \frac{V_P^2 - 2V_S^2}{2(V_P^2 - V_S^2)} \tag{7}$$

Figure 14(a) shows the relationship between normalized dynamic Poisson's ratio and irradiation time for different microwave powers, comparing the results from sandstone with results from LU et al [45]. It is indicated that experimental results are very consistent with those of LU et al. Poisson's ratio decreases with increasing irradiation time for different microwave powers, which is related to the generation of microcracks inside the rock during heating [46]. With increasing crack density, the longitudinal strain increases, which leads to the

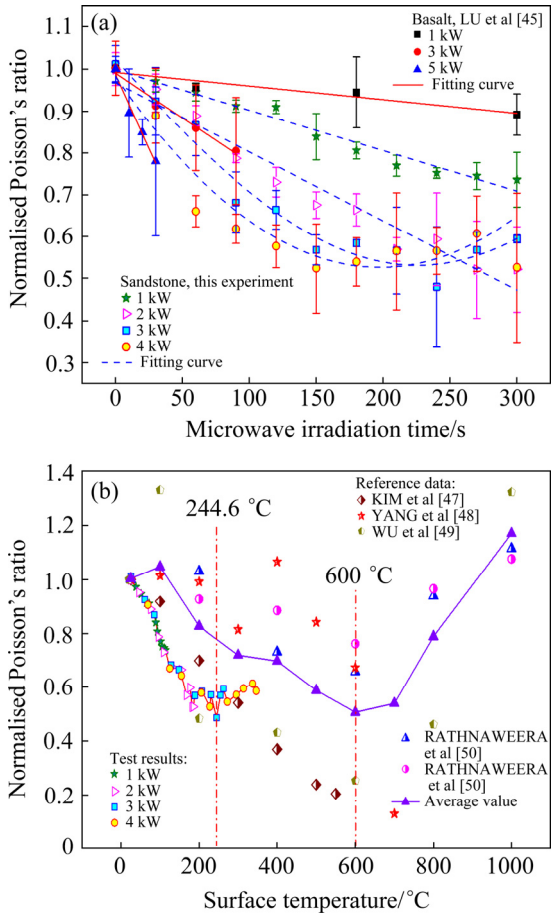

Fig. 14 Variation of Poisson's ratio of sandstone vs microwave irradiation time (a) and surface temperature (b)

decrease of Poisson's ratio. As a result, the cracks inside the rock are more likely to intersect, then shear failure occurs and rock fragments are created. However, it is worth noting that in our experiments, after the sandstone samples are exposed to 3 and 4 kW microwave power for 200 s, Poisson's ratio shows a slightly increasing trend with increasing irradiation time, which is not found by LU et al. On the other hand, Poisson's ratio has an obvious temperature dependence, so it is very instructive to consider the influence of temperature variation on Poisson's ratio.

Figure 14(b) shows the relationship between normalized Poisson's ratio and surface temperature of sandstone applying different microwave powers, in comparison with results obtained for other types of sandstone [47−50] under convective heating conditions. It becomes visible that Poisson's ratio decreases first and then increases with increasing temperature, whether it is microwave heated or convectively heated. Under convective heating conditions, Poisson's ratio of sandstone reaches its minimum value at about 600 °C. When temperature exceeds about 600 °C, Poisson's ratio begins to show an increasing trend with increasing temperature. According to the study of GREAVES et al [51], this characteristic of Poisson's ratio indicates the brittle−ductile transition. However, under microwave heating conditions, the minimum Poisson's ratio of sandstone appears at around 245 °C, which is quite different from the temperature threshold for convective heating. The reason may be the selective heating during microwave treatment. Some microwave-sensitive minerals can easily form hot spots inside the rock, and the heat dissipation from the inside to the outside of the rock is different so that significant local temperature gradients are generated, and the brittle−ductile transition may occur earlier around the microwave sensitive minerals.

4.2 Microstructure and thermal cracking mechanisms

Under the action of microwave heating, physical and mechanical properties of the rock change. This can be explained at the microscopic level by (1) local thermal stresses produced by the inhomogeneous thermal expansion of mineral particles, (2) vapor pressure produced by the vaporization of pore water, and (3) phase transformation or decomposition of mineral particles in high-temperature environment.

A scanning electron microscope (SEM) was used to observe the evolution of micro cracks on the sandstone surface with ongoing irradiation time considering different microwave irradiation powers (Fig. 15). It is found that the internal structure of sandstone is relatively intact up to about 60 s independent on microwave radiation power, and only some pores and narrow boundary cracks are found. This is due to the high sensitivity of the rock in respect to water. Under low-power microwave conditions or for short irradiation time under high microwave power, most of the microwave energy is absorbed by pore water inside the rock and used to convert water into water vapor. Under the action of steam pressure, some initial pores and intergranular fissures expand. Corresponding results are shown in Figs. 15(a, e, i, m). Additionally, the evaporation of pore water has a cooling effect on the sandstone. Therefore, within a short exposure time, the microstructure of sandstone is not change significantly.

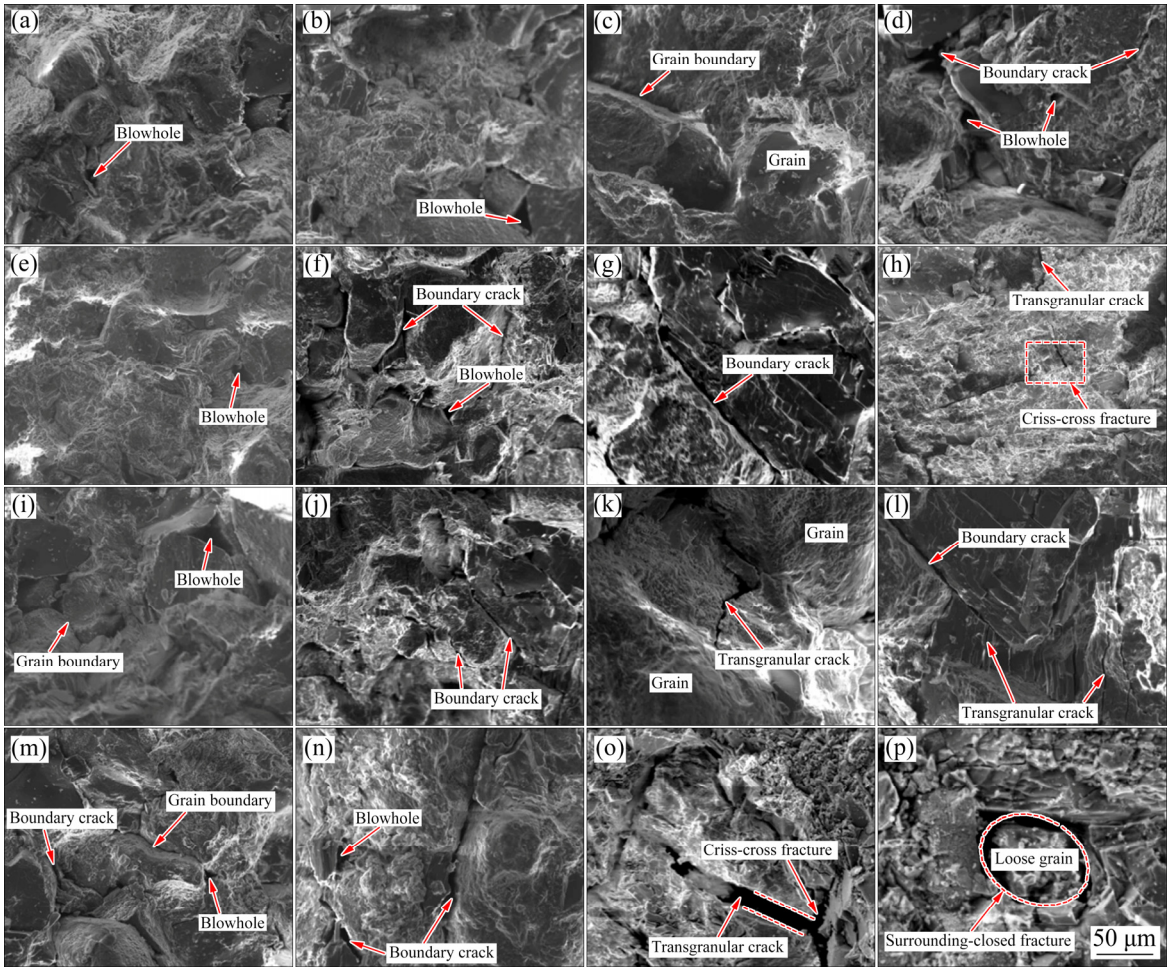

Fig. 15 SEM images of sandstone exposed to different microwave powers and irradiation time: (a) 1 kW, 60 s; (b) 1 kW, 120 s; (c) 1 kW, 180 s; (d) 1 kW, 300 s; (e) 2 kW, 60 s; (f) 2 kW, 120 s; (g) 2 kW, 180 s; (h) 2 kW, 300 s; (i) 3 kW, 60 s; (j) 3 kW, 120 s; (k) 3 kW, 180 s; (l) 3 kW, 300 s; (m) 4 kW, 60 s; (n) 4 kW, 120 s; (o) 4 kW, 180 s; (p) 4 kW, 300 s

When the microwave power is increased to 2 kW, with increasing radiation time, the number of pores increases and intergranular cracks gradually extend and open. When microwave irradiation time reaches 300 s, some adjacent cracks coalesce, as shown in Fig. 15(h). At the microwave radiation power of 3 kW, the first transgranular crack is observed, as shown in Figs. 15(k, l). When microwave power is further increased to 4 kW, many transgranular cracks become visible. With increasing radiation time, the width of transgranular cracks increases and a large number of branching cracks coalesce to form a network. Finally, a debris is produced due to the massive intersection of cracks, as shown in Fig. 15(p).

The SEM results indicate that microwave radiation causes dehydration, pore expansion and cracking. Longer duration of microwave irradiation supports the extension and opening of cracks, while increasing the microwave power is more beneficial to the generation of transcrystalline cracks and the formation of fracture networks.

Different rock forming minerals have different dielectric constants, so their sensitivity to microwaves is also different, resulting in thermal expansion and overall deformation [52]. To study the micro-mechanical mechanisms in more detail, two mineral particles A and B with different thermal expansion coefficients α_A and α_B are considered and $\alpha_B > \alpha_A$. The following basic damage processes occur (see Fig. 16):

(1) In the case that the mineral particles A and B are cemented: With increasing temperature, the particles expand and deform unevenly. The thermal strain mismatch leads to shear stress generated at the interface. The larger the difference in thermal expansion coefficient between the particles, the greater the shear stress. When the shear stress

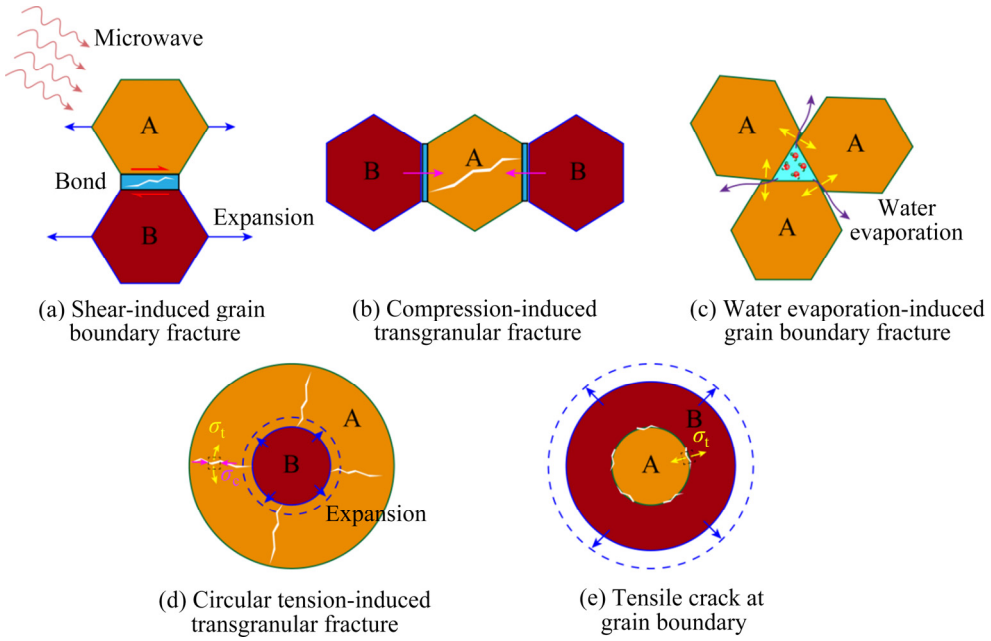

Fig. 16 Different types of crack in sandstone induced by thermal stress (Thermal expansion coefficients: $\alpha_B > \alpha_A$)

exceeds the shear strength, shear failure at the grain interface forms a boundary crack, as shown in Fig. 16(a).

(2) When particle A is sandwiched between two particles B: with increasing temperature, particle B produces large deformation and induces compressive stress. When the compressive stress exceeds the compressive strength of the particle, a transgranular crack is produced (Fig. 16(b)).

(3) Under the action of microwave heating, pore water is heated and transformed into water vapor. The corresponding gas expansion pressure acts at the pore wall, generating tangential tensile stresses [52], which eventually leads to the formation of tensile boundary cracks along weak grain boundary, as shown in Fig. 16(c).

(4) If the thermal expansion coefficient of the embedded particle is greater than that of the matrix, the embedded particle creates a radial pressure on the matrix, which is similar to the hydraulic fracturing [53]. Therefore, under the action of hoop tensile stress, the matrix mineral experiences tensile cracking, as shown in Fig. 16(d).

(5) If the thermal expansion coefficient of the embedded particles is smaller than that of the matrix, the volumetric expansion of the embedded particles is relatively small and exfoliation takes place. The maximum tensile stress occurs at the interface between matrix and embedded particles and creates tensile cracking, as shown in Fig. 16(e).

In addition to the above discussed forms of cracking, phase transformation, decomposition and melting of rock minerals in high-temperature environment are also important factors leading to the deterioration of the rock. The most typical one is $\alpha \rightarrow \beta$ quartz phase transition at 573 °C [54,55]. It can be summarized that the strength degradation process of sandstone under the action of microwave irradiation is caused by the comprehensive effects of thermal stresses, steam pressure and phase transformations of the minerals.

5 Conclusions

(1) Under the action of microwave radiation, the surface temperature of the sample shows a non-uniform distribution, which is related to the locally different heat dissipation of the rock. For different microwave irradiation powers, average surface temperature of the sandstone and radiation time follow a linear relationship.

(2) Microwave radiation can effectively weaken the physical and mechanical properties of sandstone. However, under low-power microwave conditions or for short irradiation time under high-power conditions, dynamic compressive strength and elastic modulus of the sandstone reveal a slight increase. This may be related to the partial closure

of pores and increasing interlocking caused by the thermal expansion of microwave sensitive mineral particles.

(3) With increasing microwave power and extension of radiation time, the dynamic failure mode of sandstone changes from the initial tensile failure to tensile−shear composite failure, and finally to the typical compression−shear failure, and the rock fragmentation gradually increases. The main reason for this phenomenon is the increase of crack density and the decrease of dynamic Poisson's ratio.

(4) Under the action of microwaves, thermal stresses are produced by thermal strain mismatch of different mineral particles. Vapor pressure is formed by the vaporization of pore water inside the rock, and phase transformation and decomposition of some mineral particles at high temperature are the main reasons for the deterioration of the rock.

Acknowledgments

The authors are grateful for the financial supports from the National Natural Science Foundation of China (Nos. 41972283, 11972378), the National Key Scientific Instrument and Equipment Development, China (No. 51927808), and the Hunan Provincial Innovation Foundation for Postgraduate, China (No. CX2018B066).

References

[1] LI Xi-bing, HUANG Lin-qi, ZHOU Jian, WANG Shao-feng, MA Chun-de, CHEN Jiang-zhan, LIU Zhi-xiang, LI Qi-yue, ZHAO Guo-yan. Review and prospect of mining technology in hard rock mines [J]. The Chinese Journal of Nonferrous Metals, 2019, 29: 1828−1847. (in Chinese)

[2] WANG Shao-feng, SUN Li-cheng, HUANG Lin-qi, LI Xi-bing, SHI Ying, YAO Jin-rui, DU Shao-lun. Non-explosive mining and waste utilization for achieving green mining in underground hard rock mine in China [J]. Transactions of Nonferrous Metals Society of China, 2019, 29: 1914−1928.

[3] DU K, TAO M, LI X B, ZHOU J. Experimental study of slabbing and rockburst induced by true-triaxial unloading and local dynamic disturbance [J]. Rock Mechanics and Rock Engineering, 2016, 49: 3437−3453.

[4] ROSTAMI J. Performance prediction of hard rock Tunnel Boring Machines (TBMs) in difficult ground [J]. Tunnelling and Underground Space Technology, 2016, 57: 173−182.

[5] XIA Y M, ZHANG K, LIU J S. Design optimization of TBM disc cutters for different geological conditions [J]. World Journal of Engineering and Technology, 2015, 3: 218−231.

[6] ZHENG Y L, ZHANG Q B, ZHAO J. Challenges and opportunities of using tunnel boring machines in mining [J]. Tunnelling and Underground Space Technology, 2016, 57: 287−299.

[7] CICCU R, GROSSO B. Improvement of disc cutter performance by water jet assistance [J]. Rock Mechanics and Rock Engineering, 2014, 47: 733−744.

[8] OH T M, CHO G C. Characterization of effective parameters in abrasive waterjet rock cutting [J]. Rock Mechanics and Rock Engineering, 2014, 47: 745−756.

[9] PENG X G, LI L, YANG Y F, ZHAO G L, ZENG T. Experimental study on rotary ultrasonic vibration assisted drilling rock [J]. Advances in Space Research, 2021, 67: 546−556.

[10] KOCIS I, KRISTOFIC T, GAJDOS M, HORVATH G, JANKOVIC S. Utilization of electrical plasma for hard rock drilling and casing milling [C]//SPE/IADC Drilling Conference and Exhibition. London, 2015.

[11] SHI X M, DUAN Y L, HAN B, ZHAO J. Enhanced rock breakage by pulsed laser induced cavitation bubbles: Preliminary experimental observations and conclusions [J]. Geomechanics and Geophysics for Geo-Energy and Geo-Resources, 2020, 6: 25.

[12] JERBY E, DIKHTYAR V, AKTUSHEV O, GROSGLICK U. The microwave drill [J]. Science, 2002, 298(5593): 587−589.

[13] WEI W, SHAO Z S, ZHANG Y Y, QIAO R J, GAO J P. Fundamentals and applications of microwave energy in rock and concrete processing—A review [J]. Applied Thermal Engineering, 2019, 157: 113751.

[14] LU G M, FENG X T, LI Y H, ZHANG X W. The microwave-induced fracturing of hard rock [J]. Rock Mechanics and Rock Engineering, 2019, 52: 3017−3032.

[15] GUSHCHIN V V, KUZNETSOV V V, CHERNIKOV V A, MERZON A G, PROTASOV Y I, VARTANOV G A. Driving horizontal workings by means of an entry drifting machine with electrothermomechanical cutting [J]. Soviet Mining, 1979, 15: 133−137.

[16] PROTASOV Y I, KUZNETSOV V V, MERZON A G, CHERNIKOV V A, RETINSKII V S. A study of electrothermomechanical destruction of hard rocks with a rotary heading machine [J]. Soviet Mining, 1984, 20: 462−467.

[17] HASSANI F, NEKOOVAGHT P M, GHARIB N. The influence of microwave irradiation on rocks for microwave-assisted underground excavation [J]. Journal of Rock Mechanics and Geotechnical Engineering, 2016, 8: 1−15.

[18] SATISH H, OUELLET J, RAGHAVAN V, RADZISZEWSKI P. Investigating microwave assisted rock breakage for possible space mining applications [J]. Mining Technology, 2006, 115: 34−40.

[19] KAHRAMAN S, CANPOLAT A N, FENER M. The influence of microwave treatment on the compressive and tensile strength of igneous rocks [J]. International Journal of Rock Mechanics and Mining Sciences, 2020, 129: 104303.

[20] NEJATI H, HASSANI F, RADZISZEWSKI P. Experimental investigating of fracture toughness reduction and fracture development in basalt specimens under microwave illumination [C]//Proceeding of Earth and Space Conference. California, 2012: 325−334.

[21] GE Z L, SUN Q, XUE L, YANG T. The influence of microwave treatment on the mode I fracture toughness of

granite [J]. Engineering Fracture Mechanics, 2021, 249: 107768.

[22] SHEPEL T, GRAFE B, HARTLIEB P, DREBENSTEDT C, MALOVYK A. Evaluation of cutting forces in granite treated with microwaves on the basis of multiple linear regression analysis [J]. International Journal of Rock Mechanics and Mining Sciences, 2018, 107: 69−74.

[23] ALI A Y, BRADSHAW S M. Bonded-particle modelling of microwave-induced damage in ore particles [J]. Minerals Engineering, 2010, 23: 780−790.

[24] BATCHELOR A R, JONES D A, PLINT S, KINGMAN S W. Deriving the ideal ore texture for microwave treatment of metalliferous ores [J]. Minerals Engineering, 2015, 84: 116−129.

[25] KINGMAN S W. Recent developments in microwave processing of minerals [J]. International Materials Reviews, 2006, 51: 1−12.

[26] ZHENG Y L, ZHANG Q B, ZHAO J. Effect of microwave treatment on thermal and ultrasonic properties of gabbro [J]. Applied Thermal Engineering, 2017, 127: 359−369.

[27] DAI J, SONG S D, TU B B, GAO Y Z, DU W P. Influence of granite strength under different microwave irradiation parameters [J]. Science Technology and Engineering 2017, 17(18): 1671−1815. (in Chinese)

[28] SUN W, LING J X, HUO J Z, GUO L, ZHANG X, DENG L Y. Dynamic characteristics study with multidegree-of-freedom coupling in TBM cutterhead system based on complex factors [J]. Mathematical Problems in Engineering, 2013: 635809.

[29] LI X B, GONG F Q. Research progress and prospect of deep rock mechanics based on coupled static dynamic loading testing [J]. Journal of China Coal Society, 2021, 6(3): 846−866. (in Chinese)

[30] LI X B, LOK T S, ZHAO J. Dynamic characteristics of granite subjected to intermediate loading rate [J]. Rock Mechanics and Rock Engineering, 2005, 38: 21−39.

[31] KINGMAN S W, JACKSON K, BRADSHAW S M, ROWSON N A, GREENWOOD R. An investigation into the influence of microwave treatment on mineral ore comminution [J]. Powder Technology, 2004, 146: 176−184.

[32] RIZMANOSKI V. The effect of microwave pretreatment on impact breakage of copper ore [J]. Minerals Engineering, 2011, 24: 1609−1618.

[33] ZHU Y Q, DAI J, YUN F F, ZHAI H H, ZHANG M, FENG L R. Dynamic response and fracture characteristics of granite under microwave irradiation [J]. Journal of Mining and Strata Control Engineering, 2022, 4(1): 019921. (in Chinese)

[34] WANG S, XU Y, XIA K W, TONG T Y. Dynamic fragmentation of microwave irradiated rock [J]. Journal of Rock Mechanics and Geotechnical Engineering, 2021, 13(2): 300−310.

[35] LU G M, ZHOU J J, LI Y H, ZHANG X W, CAO W Y. The influence of minerals on the mechanism of microwave-induced fracturing of rocks [J]. Journal of Applied Geophysics, 2020, 180: 104123.

[36] LI Q, LI X B, YIN T B. Effect of microwave heating on fracture behavior of granite: An experimental investigation [J]. Engineering Fracture Mechanics, 2021, 250: 107758.

[37] GE Z L, SUN Q. Acoustic emission characteristics of gabbro after microwave heating [J]. International Journal of Rock Mechanics and Mining Sciences, 2021, 138: 104616.

[38] ZHAO Q H, ZHAO X B, ZHENG Y L, LI J C, HE L, HE J L, ZOU C J. Heating characteristics of igneous rock-forming minerals under microwave irradiation [J]. International Journal of Rock Mechanics and Mining Sciences, 2020, 135: 104519.

[39] ZHOU Y X, XIA K W, LI X B, LI H B, MA G W, ZHAO J, ZHOU Z L, DAI F. Suggested methods for determining the dynamic strength parameters and mode-I fracture toughness of rock materials [J]. International Journal of Rock Mechanics and Mining Sciences, 2012, 49: 105−112.

[40] LI X B, ZOU Y, ZHOU Z L. Numerical simulation of the rock SHPB test with a special shape striker based on the discrete element method [J]. Rock Mechanics and Rock Engineering, 2014, 47: 1693−1709.

[41] ZHANG Q B, ZHAO J. A review of dynamic experimental techniques and mechanical behaviour of rock materials [J]. Rock Mechanics and Rock Engineering, 2014, 47: 1411−1478.

[42] WANG P, YIN T B, LI X B, HU B W. Dynamic tensile strength and failure mechanisms of thermally treated sandstone under dry and water-saturated conditions [J]. Transactions of Nonferrous Metals Society of China, 2020, 30: 2217−2238.

[43] LU G M, LI Y H, HASSANI F, ZHANG X W. The influence of microwave irradiation on thermal properties of main rock-forming minerals [J]. Applied Thermal Engineering, 2017, 112: 1523−1532.

[44] ZHU X J. Hydraulic properties of soft rock [J]. Mining Engineering Technology, 1996, 3: 46−50. (in Chinese)

[45] LU G M, FENG X T, LI Y H, ZHANG X W. Influence of microwave treatment on mechanical behaviour of compact basalts under different confining pressures [J]. Journal of Rock Mechanics and Geotechnical Engineering, 2020, 12: 213−222.

[46] WALSH J. The effect of cracks in rocks on Poisson's ratio [J]. Journal of Geophysical Research, 1965, 70: 5249−5257.

[47] KIM B C, CHEN J, KIM J Y. Relation between crack density and acoustic nonlinearity in thermally damaged sandstone [J]. International Journal of Rock Mechanics and Mining Sciences, 2020, 125: 104171.

[48] YANG S Q, RANJITH P G, JING H W, TIAN W L, JU Y. An experimental investigation on thermal damage and failure mechanical behavior of granite after exposure to different high temperature treatments [J]. Geothermics, 2017, 65: 180−197.

[49] WU G, WANG Y, SWIFT G, CHEN J. Laboratory investigation of the effects of temperature on the mechanical properties of sandstone [J]. Geotechnical and Geological Engineering, 2013, 31: 809−816.

[50] RATHNAWEERA T D, RANJITHA P G, GU X, PERERAA M S A, KUMARI W G P, WANNIARACHCHI W A M, HAQUE A, LI J C. Experimental investigation of thermomechanical behaviour of clay-rich sandstone at extreme temperatures followed by cooling treatments [J]. International Journal of Rock Mechanics and Mining Sciences, 2018, 107: 208−223.

[51] GREAVES G N, GREER A, LAKES R, ROUXEL T. Poisson's ratio and modern materials [J]. Nature Materials, 2011, 10: 823−837.
[52] KIM S, SANTAMARINA J C. Rock crushing using microwave pre-treatment [C]//Proceedings of the Geo-Chicago 2016. Chicago, Illinois, USA, 2016: 720−729.
[53] TANG S B, TANG C A, ZHU W C, WANG S H, YU Q L. Numerical investigation on rock failure process induced by thermal stress [J]. Chinese Journal of Rock Mechanics and Engineering, 2006, 25: 2071−2078. (in Chinese)
[54] HEUZE F E. High-temperature mechanical, physical and thermal properties of granitic rocks — A review [J]. International Journal of Rock Mechanics and Mining Sciences & Geomechanics Abstracts, 1983, 20: 3−10.
[55] WANG F, KONIETZKY H. Thermo-mechanical properties of granite at elevated temperatures and numerical simulation of thermal cracking [J]. Rock Mechanics and Rock Engineering, 2019, 52: 3737−3755.

中等加载速率下微波损伤砂岩的动态抗压强度及破坏机理

王 品[1,2]，尹土兵[1]，李夕兵[1]，Heinz KONIETZKY[2]

1. 中南大学 资源与安全工程学院，长沙 410083；
2. Geotechnical Institute, TU Bergakademie Freiberg, Freiberg, 09596, Germany

摘 要：为了研究微波加热对岩石动态特性和破坏机制的影响，使用改进的分离式霍普金森压杆系统对微波辐射砂岩试样进行动态压缩试验。结果表明，微波辐射能有效降低砂岩的抗压强度。冲击荷载作用下试样呈现出 3 种不同的破坏模式：拉伸破坏、拉伸−剪切复合破坏和压缩−剪切破坏。利用实测的纵、横波速度计算得到的动态泊松比来描述砂岩的变形特征。随着微波功率和加热时间的增加，泊松比先下降后略有增加，转折点温度出现在 244.6 ℃。 此外，微观结构特征表明，微波辐射对岩石产生脱水、扩孔和致裂效应。基于岩石内部热应力和蒸汽压力，探讨微波辐射对岩石的损伤机理，为实验结果提供合理的解释。

关键词：砂岩；微波辐射；热裂；动态抗压强度；破坏模式；分离式霍普金森压杆

(Edited by Bing YANG)